8A.5 THE INITIATION, LONGEVITY AND MORPHOLOGY OF SIMULATED CONVECTIVE STORMS AS A FUNCTION OF FREE TROPOSPHERIC RELATIVE HUMIDITY

Eugene W. McCaul, Jr.*, and Charles Cohen
Universities Space Research Association
Huntsville, Alabama

1. INTRODUCTION

McCaul and Cohen (2002; hereinafter MC02) proposed an eight dimensional parameter space as a simplified framework for describing the basic behavior of deep convective storms. McCaul and Weisman (2001; MW01) explored two of these dimensions, namely the shapes of the parcel buoyancy and the environmental vertical shear profiles. MC02 explored two other parameters, the depths of the mixed and moist layers, equivalent in their experiment design to the lifted condensation level (LCL) and the level of free convection (LFC). More recently, McCaul et al. (2004; MCK04) reported on the sensitivity of simulated storms to another parameter, the temperature at the LCL, which is closely related to the environmental precipitable water (PW), with warmer LCL temperatures associated with larger PW.

As the parameter space envisioned by MC02 continues to be explored, one other key parameter, the free tropospheric relative humidity (FTRH), has come under scrutiny. In MW01, MC02 and MCK04, the FTRH was always set to 90%. Here we examine the behavior of simulated storms in environments having a series of different, smaller values of FTRH.

It is important to note that all the environments studied here feature FTRH initial profiles that are constant from the LFC to the tropopause. This differs from the approach taken by Gilmore and Wicker (1998), who examined the effect of shallow lower-tropospheric dry layers inserted into a single sounding. While such an approach is useful, and our model reproduces their general findings when initialized in a manner similar to theirs, there has been surprisingly little systematic numerical simulation research into the impact of differing values of FTRH on convective storms. The parameter space approach proposed by MC02 provides a way of accomplishing such research in a controlled way, such that all other environmental parameters are maintained constant. Thus, in the simulations reported here, we can examine not only the effects of different values of FTRH, but also the differences in those effects as other environmental parameters assume different combinations within the full parameter space.

Intuition and experience both suggest that drier midtropospheric environments tend to hinder deep convection. In discussing the behavior of tropical convection, Raymond (1995) concludes that dry air aloft is likely to hinder deep convective storm development, even when convective available potential energy (CAPE) is abundant. One important mechanism in moistening the midtroposphere is mixing and detrainment from cumulus clouds, as described by Perry and Hobbs (1996). It seems obvious that one way to convert a dry, unstable environment unsupportive of deep convection into a more moist unstable one that does support deep convection is for shallow convection to start the moistening process from the bottom up, allowing for increasingly deep convective towers to develop subsequently.

In the case of midlatitude convection, the picture is more complex than in the tropics because of the presence of large horizontal gradients, but some of the same physical mechanisms are at work. For example, there are many observed soundings that seem to indicate an abundance of dry air aloft in the vicinity of severe storms. However, in many of these cases, the midtropospheric dryness is accompanied by extremely steep low-level lapse rates and large CAPE, both of which have been shown to promote vigorous convection (see MW01 and Weisman and Klemp 1982; 1984). In such cases, it is not obvious exactly which environmental characteristic is most important in regulating storm intensity and longevity. Furthermore, the validity of such very dry soundings as true proximity soundings relevant to the severe convection could be questioned based on many observational studies that emphasize the importance of the horizontal inhomogeneities acting on small scales.

Another potentially important factor to consider is that very moist soundings might ultimately prevent realization of the strongest convective overturning, because of an excessive proliferation of updrafts that necessarily compete for the available energy supply of low-level moisture. Thus, it is possible that storms with the highest possible overturning efficiency (see MW01, MC02) might occur in environments that are neither too dry nor too close to saturation. The purpose of this research is to untangle all these effects and determine how storms might actually behave in idealized environments of varying FTRH.

2. METHODOLOGY

In the experiments reported here, we use the Regional Atmospheric Modeling System (RAMS), version 3b (Pielke *et al.* 1992; Walko *et al.* 1995), with additional modifications described in MCK04.

**Corresponding author address*: Eugene W. McCaul, Jr., Universities Space Research Association, 6700 Corporate Drive, Suite 203, Huntsville, AL 35806, E-mail: mccaul@space.hsv.usra.edu

Although three CAPE regimes were examined, we limit discussion here to the CAPE=2000 J kg^{-1} results, which appear to be representative of what happens in environments capable of supporting severe convection. Because the simulations represent a portion of an eight-dimensional parameter space study, an experiment nomenclature consisting of eight pairs of alphabetic and numeric characteris has been devised, as documented in MCK04. For a comprehensive description of the nomenclature and how to decode each experiment's name, the reader is referred to our website at http://space.hsv.usra.edu/COMPASS. In brief, the nomenclature's eight parameter identifiers are e for CAPE (*e2* implies CAPE=2000 J kg^{-1}), c for radius of a curved hodograph (*c2* implies a radius of 12 m s^{-1}), m for buoyancy profile compression (large m implies large low-level lapse rates), n for shear profile compression (behaves like m), k for model level nearest the LCL, f for model level nearest the LFC, p for LCL temperature or, approximately, environmental precipitable water (PW), and h for FTRH. In these experiments, we study how convection behaves as h changes, all seven other parameters held fixed, for a variety of vectors of the other seven parameters. In previously reported results, we employed an h value designated as *h9*, implying 90% FTRH. Here we extend the work to include FTRH values of 80%, 70% and 60%. This range of values appears to be sufficient to describe how storms vary as FTRH varies.

All simulations are conducted on a 75 x 75 km grid having horizontal mesh resolution of 500 m. The vertical mesh is stretched, with low-level resolution of 250 m and a lowest model level of 127 m above the surface, and resolution at 20 km altitude of 750 m. A 4.5 km deep sponge layer is placed above 20 km altitude to absorb stratospheric gravity waves. Default choices are employed for all microphysical species size distribution parameters, and subgrid turbulence effects are handled using an isotropic, three-dimensional deformation based scheme. Full model fields are saved every 5 min for postanalysis.

Convection is initiated using circularly symmetric bubbles vertically centered at the surface. The amplitudes of the bubbles in the CAPE=2000 J kg^{-1} simulations are normally 1.5K for the warmer (PW=6 cm) cases, and 2.0K for the cooler (PW=3 cm) cases, which gives starting impulses with roughly similar equivalent potential temperature perturbation amplitudes. However, as will be shown, systematic increases in bubble amplitude are often needed to trigger deep convective storms as FTRH decreases.

In constructing our starting profiles, we were careful to ensure that the profiles of virtual temperature were held constant in the free troposphere when the FTRH was changed. Thus, our dry soundings (Fig. 1) feature a small inversion in ordinary temperature just above the LFC, which is not noticeable in our default 90% FTRH sounding.

3. RESULTS AND DISCUSSION

The simulations reveal that reduction in FTRH consistently leads to fewer deep convective cells, with negligible activity after 2 h of simulated time when FTRH drops below 60%, if the default warm bubble amplitudes listed earlier are used. To see how the convection behaves if the warm bubbles are made warmer, we performed additional simulations with starting bubbles 0.5°C, 1.0°C, 1.5°C and 2.0°C warmer than the default. The warmest bubbles used were thus only 4.0°C in amplitude, which is within the limits of what is commonly used by the storm modeling community for most case study work, and seems reasonable for simulations where CAPE values are 2000 J kg^{-1}.

The use of increasingly warm starting bubbles allows for some of the lower FTRH storm environments to sustain deeper or more persistent convection, but the driest environmental FTRH values still tend to suppress convection late in the simulations. Fig. 2 shows maps of domain-wide convective activity at t = 120 min for the high-LCL, high-LFC, low-PW *e2c2m4n4k6f6p3* case, as a function of varying FTRH (i.e., *h6*, *h7*, *h8* and *h9*), with starting bubble amplitudes augmented by 0.5K for each 10% reduction in FTRH below the default of 90%. The default *h9* simulation is shown at the upper right, and it clearly exhibits more widespread convection than the other simulations in the figure. For *h8* (upper left panel), both left-moving and right-moving storm components are maintained, but with fewer weak cells around and between the principal cells. In the case of *h7* (lower right panel), the left-mover is still substantial, but the right-mover has just dissipated. At *h6* (lower left panel), only a rather weak left-mover is evident, with no hint of a right-mover remaining.

It is of interest to see how the persistent right-mover in the *h8* case compares with the right-mover in the default *h9* simulation. Fig. 3 shows the time series of peak updraft velocities w_{max} in the right moving storms from Fig. 2. The figure reveals that the w_{max} for the *h8* case does indeed rival that of the default *h9* case; in fact, the largest w_{max} for the *h8* case slightly exceeds that of *h9*, although the latter maintains a larger average peak updraft. Fig. 3 also shows that w_{max} for the drier *h7* and *h6* cases is much smaller, with the *h6* right-mover dissipating by about t = 90 min, and the *h7* case lasting about 30 min longer. Fig. 4 reveals that these decreases in peak updraft speed are also accompanied by reduced updraft cross-sectional area.

The deleterious effects of reduced FTRH evident in the high-LCL, high-LFC, storms in Fig. 2 are even more pronounced in low-LCL, low-LFC environments (not shown). In these latter cases, there is no sustained convection at t = 120 min for either the *h6* or *h7* cases, and the *h8* case consists of only a weakened left-mover. Results from the low-LCL, high-LFC simulations (also not shown) reveal an intermediate level of sensitivity to reductions in FTRH, but with the interesting twist that the right-movers exhibit greater survivability than the left-movers.

The mechanism for diminished storm survival when FTRH is reduced is clearly entrainment of dry air by the growing storm towers (see Stommel 1947; Squires 1958). The effect of the dry air is to promote excessive amounts of evaporative cooling, and attendant reduction of updraft buoyancy, in the early stages of updraft growth. Time series of surface cold pool temperature under the storms (not shown) clearly reveal premature development of the cold pool. Ironically, the cold pool temperatures later in the simulations are not particularly cold, primarily because the premature cold pool development has such a strong suppressive effect on the early phase of the convective cell's life cycle. The impact of the reduced FTRH is much stronger for low-LCL, low-LFC storms because of their tendency to have narrower updrafts that are more susceptible to environmental dilution (see MC02), while the high LFC storms are slower to succumb to the effects of mixing with the dry air.

4. SUMMARY AND OUTLOOK

From these simulations, it appears that FTRH values of 70% and lower have a well-defined negative impact on convective cell vigor and survivability. This is consistent with the findings of many observational studies of convection, which generally show that in dry environments, storms must bubble for some time within a mesoscale zone of low-level convergence and ascent, thus preconditioning the atmosphere, before persistent deep convection can develop and survive. It also suggests that soundings featuring deep layers of low humidity aloft, even east of fronts and drylines, are likely not truly representative of the conditions near storms if those storms show survivability of more than 2 h. On the other hand, environments having sufficient CAPE, such as those discussed here, evidently have no difficulty producing brief, strong pulse-type convective storms when FTRH is reduced.

Future work should explore these FTRH-related sensitivities in more detail. In particular, because mixing processes are so strongly implicated in these findings, we recommend additional sensitivity studies involving the model microphysics and turbulence parameterizations. This should include use of finer model meshes for improved representation of small-scale mixing processes.

5. REFERENCES

Gilmore, M. S., and L. J. Wicker, 1998: The influence of midtropospheric dryness on supercell morphology and evolution. *Mon. Wea. Rev.*, **126**, 943–958.

McCaul, E. W., Jr., and C. Cohen, 2002: The impact on simulated storm structure and intensity of variations in the mixed layer and moist layer depths. *Mon. Wea. Rev.*, **130**, 1722–1748.

——, ——, and C. Kirkpatrick, 2004: The sensitivity of simulated storm structure and intensity to the temperature at the lifted condensation level. submitted to *Mon. Wea. Rev.*

McCaul, E. W., Jr., and M. L. Weisman, 2001: The sensitivity of simulated supercell structure and intensity to variations in the shapes of environmental buoyancy and shear profiles. *Mon. Wea. Rev.*, **129**, 664–687.

Perry, K. D., and P. V. Hobbs, 1996: Influences of isolated cumulus clouds on the humidity of their surroundings. *J. Atmos. Sci.*, **53**, 159–174.

Pielke, R. A., W. R. Cotton, R. L. Walko, C. J. Tremback, W. A. Lyons, L. D. Grasso, M. E. Nicholls, M. D. Moran, D. A. Wesley, T. J. Lee, and J. H. Copeland, 1992: A comprehensive meteorological modeling system - RAMS. *Meteor. Atmos. Phys.*, **49**, 69–91.

Raymond, D. J., 1995: Regulation of moist convection over the West Pacific warm pool. *J. Atmos. Sci.*, **52**, 3945–3959.

Squires, P., 1958: Penetrative downdraughts in cumuli. *Tellus*, **10**, 381–389.

Stommel, H., 1947: Entrainment of air into a cumulus cloud. *J. Meteor.*, **4**, 91–94.

Walko, R. L., W. R. Cotton, M. P. Meyers, and J. Y. Harrington, 1995: New RAMS cloud microphysics parameterization. Part I: The single-moment scheme. *Atmos. Res.*, **38**, 29–62.

Weisman, M. L., and J. B. Klemp, 1982: The dependence of numerically simulated convective storms on vertical wind shear and buoyancy. *Mon. Wea. Rev.*, **110**, 504–520.

Weisman, M. L., and J. B. Klemp, 1984: The structure and classification of numerically simulated convective storms in directionally varying shears. *Mon. Wea. Rev.*, **112**, 2479–2498.

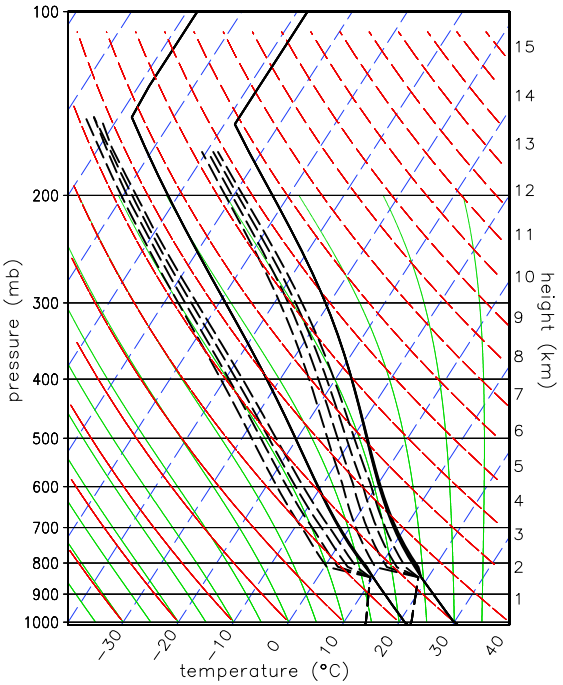

Fig. 1. Skew T-log p diagrams of starting temperature and dewpoint profiles for the e2c2m4n4k6f6p3hx experiments (left side of chart) and e2c2m4n4k6f6p6hx experiments (right side) described in the text. Here the free tropospheric relative humidity parameter h assumes values that correspond, from right to left within each series of dewpoint curves, to 90%, 80%, 70% and 60% relative to water or ice, respectively, as ambient temperatures dictate.

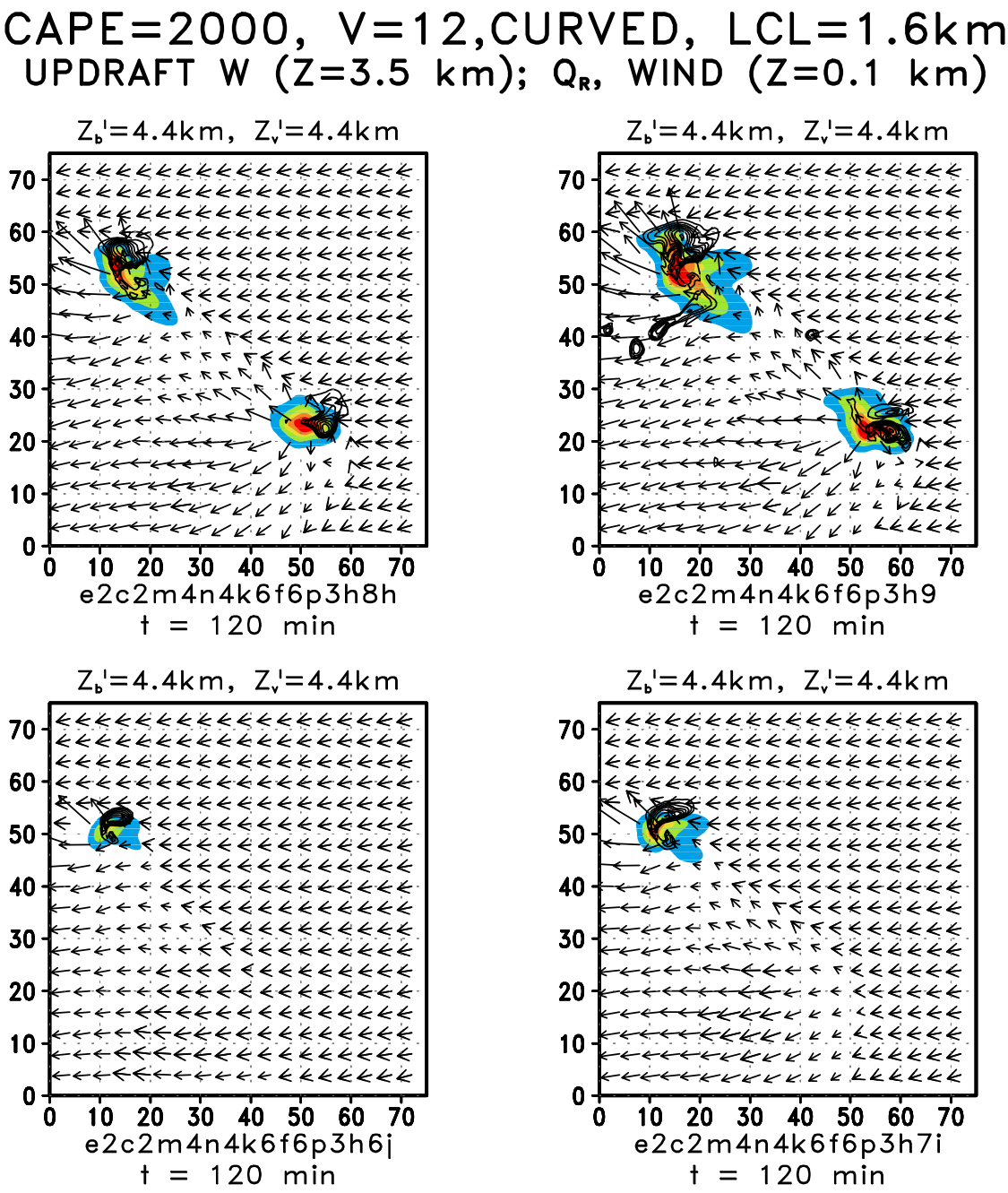

Fig. 2. Sample of maps of domain-wide array of simulated storms at t = 120 min for the e2c2m4n4k6f6p3hx cases, where x assumes the values (9, 8, 7, 6), corresponding to environmental humidity values of (90%, 80%, 70%, 60%). Shaded fields are near-surface rain mixing ratio, shaded at 0.25, 1.0, 2.0, 3.0 and 4.0 g kg^{-1} intervals, while solid contours represent updraft speed at 3.5 km altitude, with contours at 2 m s^{-1} intervals. Near-surface ground-relative wind vectors are also displayed, with larger vector heads representing temperatures comparable to undisturbed inflow, and smaller heads representing rain-cooled outflow. Experiment name suffixes (h, i, j) denote enhanced warm bubble amplitudes of (2.5, 3.0, 3.5)° C, respectively, used for the driest three simulation cases.

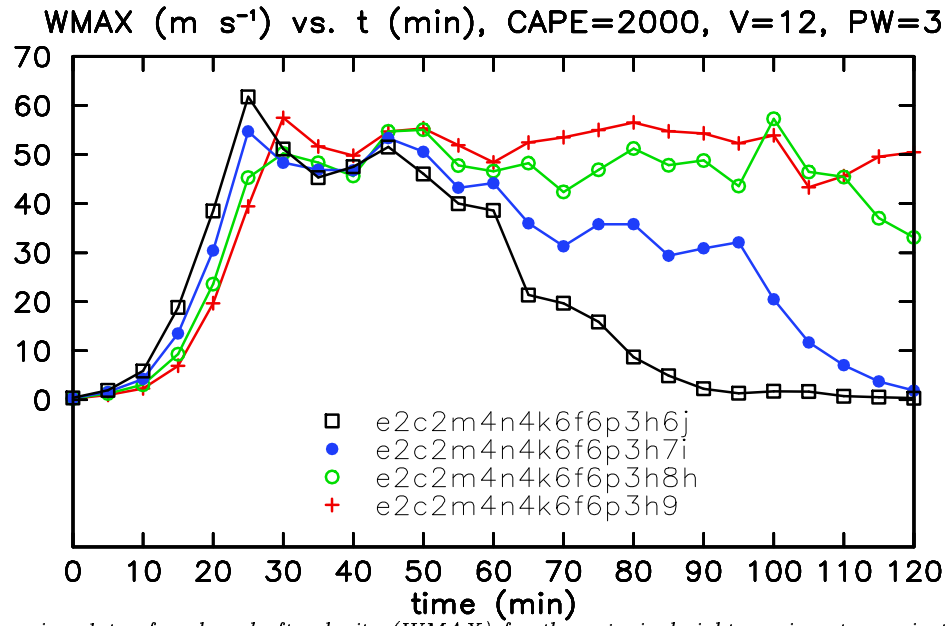

Fig. 3. Time series plots of peak updraft velocity (WMAX) for the principal right-moving storms in the simulations presented in Fig. 2.

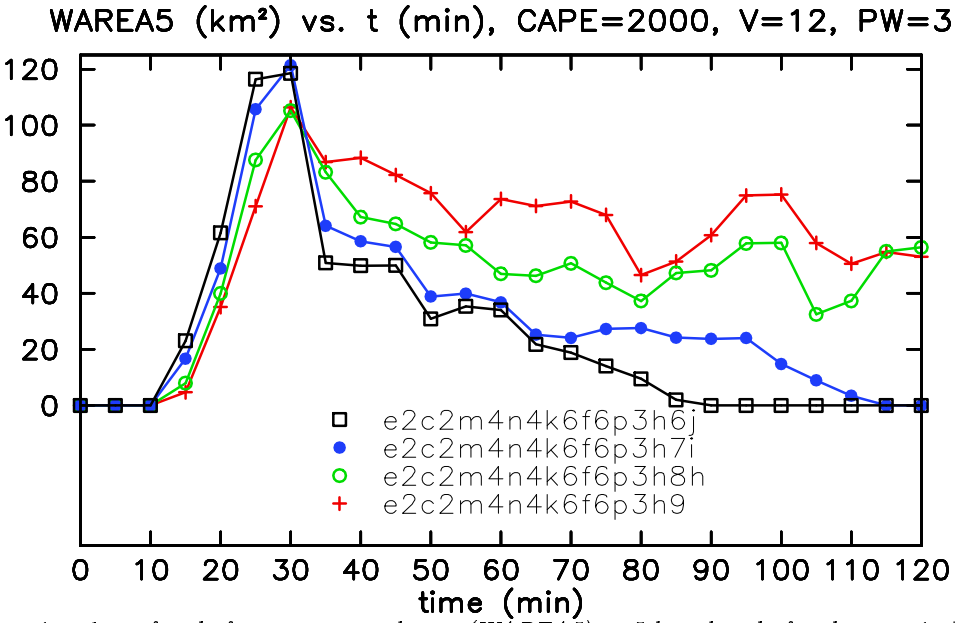

Fig. 4. Time series plots of updraft cross-sectional area (WAREA5) at 5 km altitude for the principal right-moving storms in the simulations presented in Fig. 2.